Structural control of nonlinear optical absorption and refraction in dense metal nanoparticle arrays

Dana C. Kohlgraf-Owens[1] and Pieter G. Kik[1,2,*]

[1]*CREOL, The College of Optics and Photonics, University of Central Florida, 4000 Central Florida Blvd, Orlando, FL 32816, USA*
[2]*Department of Physics, University of Central Florida, 4000 Central Florida Blvd, Orlando, FL 32816, USA*
** kik@creol.ucf.edu*

Abstract: The linear and nonlinear optical properties of a composite containing interacting spherical silver nanoparticles embedded in a dielectric host are studied as a function of interparticle separation using three dimensional frequency domain simulations. It is shown that for a fixed amount of metal, the effective third-order nonlinear susceptibility of the composite $\chi^{(3)}(\omega)$ can be significantly enhanced with respect to the linear optical properties, due to a combination of resonant surface plasmon excitation and local field redistribution. It is shown that this geometry-dependent susceptibility enhancement can lead to an improved figure of merit for nonlinear absorption. Enhancement factors for the nonlinear susceptibility of the composite are calculated, and the complex nature of the enhancement factors is discussed.

©2009 Optical Society of America

OCIS codes: (260.2065) Effective medium theory; (160.1245) Artificially engineered materials; (160.4330) Nonlinear optical materials; (160.4236) Nanomaterials.

References and links

1. C. M. Soukoulis, S. Linden, and M. Wegener, "Physics. Negative refractive index at optical wavelengths," Science **315**(5808), 47–49 (2007).
2. R. A. Shelby, D. R. Smith, and S. Schultz, "Experimental verification of a negative index of refraction," Science **292**(5514), 77–79 (2001).
3. H. J. Lezec, J. A. Dionne, and H. A. Atwater, "Negative refraction at visible frequencies," Science **316**(5823), 430–432 (2007).
4. J. B. Pendry, D. Schurig, and D. R. Smith, "Controlling electromagnetic fields," Science **312**(5781), 1780–1782 (2006).
5. D. Schurig, J. J. Mock, B. J. Justice, S. A. Cummer, J. B. Pendry, A. F. Starr, and D. R. Smith, "Metamaterial electromagnetic cloak at microwave frequencies," Science **314**(5801), 977–980 (2006).
6. K. Tsuchiya, S. Nagayasu, S. Okamoto, T. Hayakawa, T. Hihara, K. Yamamoto, I. Takumi, S. Hara, H. Hasegawa, S. Akasaka, and N. Kosikawa, "Nonlinear optical properties of gold nanoparticles selectively introduced into the periodic microdomains of block copolymers," Opt. Express **16**(8), 5362–5371 (2008).
7. J. E. Sipe, and R. W. Boyd, "Nonlinear susceptibility of composite optical materials in the Maxwell Garnett model," Phys. Rev. A **46**(3), 1614–1629 (1992).
8. M. I. Stockman, K. B. Kurlayev, and T. F. George, "Linear and nonlinear optical susceptibilities of Maxwell Garnett composites: Dipolar spectral theory," Phys. Rev. B **60**(24), 17071–17083 (1999).
9. D. Stroud, and P. M. Hui, "Nonlinear susceptibilities of granular matter," Phys. Rev. B **37**(15), 8719–8724 (1988).
10. H. Ditlbacher, N. Felidj, J. R. Krenn, B. Lamprecht, A. Leitner, and F. R. Aussenegg, "Electromagnetic interaction of fluorophores with designed two-dimensional silver nanoparticle arrays," Appl. Phys. B **73**(4), 373–377 (2001).
11. A. M. Glass, A. Wokaun, J. P. Heritage, J. G. Bergman, P. F. Liao, and D. H. Olson, "Enhanced two-photon fluorescence of molecules adsorbed on silver particle films," Phys. Rev. B **24**(8), 4906–4909 (1981).
12. W. Wenseleers, F. Stellacci, T. Meyer-Friedrichsen, T. Mangel, C. A. Bauer, S. J. K. Pond, S. R. Marder, and J. W. Perry, "Five Orders-of-Magnitude Enhancement of Two-Photon Absorption for Dyes on Silver Nanoparticle Fractal Clusters," J. Phys. Chem. B **106**(27), 6853–6863 (2002).
13. X. Hu, P. Jiang, C. Ding, H. Yang, and Q. Gong, "Picosecond and low-power all-optical switching based on an organic photonic-bandgap microcavity," Nat. Photonics **2**(3), 185–189 (2008).
14. R. Katouf, T. Komikado, M. Itoh, T. Yatagai, and S. Umegaki, "Ultra-fast optical switches using 1D polymeric photonic crystals," Photonics Nanostruct. Fundam. Appl. **3**(2-3), 116–119 (2005).

#112341 - $15.00 USD Received 3 Jun 2009; revised 5 Aug 2009; accepted 6 Aug 2009; published 10 Aug 2009

15. M. Scalora, J. P. Dowling, C. M. Bowden, and M. J. Bloemer, "Optical limiting and switching of ultrashort pulses in nonlinear photonic band gap materials," Phys. Rev. Lett. **73**(10), 1368–1371 (1994).
16. D. C. Kohlgraf-Owens, and P. G. Kik, "Numerical study of surface plasmon enhanced nonlinear absorption and refraction," Opt. Express **16**(14), 10823–10834 (2008).
17. G. Piredda, D. D. Smith, B. Wendling, and R. W. Boyd, "Nonlinear optical properties of a gold-silica composite with high gold fill fraction and the sign change of its nonlinear absorption coefficient," J. Opt. Soc. Am. B **25**(6), 945–950 (2008).
18. H. B. Liao, W. Wen, and G. K. L. Wong, "Preparation and characterization of Au/SiO_2 multilayer composite films with nonspherical Au particles," Appl. Phys., A Mater. Sci. Process. **80**(4), 861–864 (2005).
19. N. Pinçon, B. Palpant, D. Prot, E. Charron, and S. Debrus, "Third-order nonlinear optical response of Au:SiO_2 thin films: Influence of gold nanoparticle concentration and morphologic parameters," Eur. Phys. J. D **19**, 395–402 (2002).
20. O. Maruyama, Y. Senda, and S. Omi, "Non-linear optical properties of titanium dioxide films containing dispersed gold particles," J. Non-Cryst. Solids **259**(1-3), 100–106 (1999).
21. G. Ma, W. Sun, S.-H. Tang, H. Zhang, Z. Shen, and S. Qian, "Size and dielectric dependence of the third-order nonlinear optical response of Au nanocrystals embedded in matrices," Opt. Lett. **27**(12), 1043–1045 (2002).
22. J. Jayabalan, A. Singh, R. Chari, and S. M. Oak, "Ultrafast third-order nonlinearity of silver nanospheres and nanodiscs," Nanotechnology **18**(31), 315704 (2007).
23. O. Levy, and D. Stroud, "Maxwell Garnett theory for mixtures of anisotropic inclusions: Application to conducting polymers," Phys. Rev. B **56**(13), 8035–8046 (1997).
24. J. C. M. Garnett, ""Colours in Metal Glasses and in Metallic Films," Philos. Trans. R. Soc. London Ser. A **203**(1), 385–420 (1904).
25. H. R. Ma, R. F. Xiao, and P. Sheng, "Third-order optical nonlinearity enhancement through composite microstructures," J. Opt. Soc. Am. B **15**(3), 1022–1029 (1998).
26. R. del Coso, and J. Solis, "Relation between nonlinear refractive index and third-order susceptibility in absorbing media," J. Opt. Soc. Am. B **21**(3), 640–644 (2004).
27. P. B. Johnson, and R. W. Christy, "Optical-Constants Of Noble-Metals," Phys. Rev. B **6**(12), 4370–4379 (1972).
28. Microwave Studio, Computer Simulation Technology, Darmstadt, Germany.
29. S. A. Maier, P. G. Kik, and H. A. Atwater, "Observation of coupled plasmon-polariton modes in Au nanoparticle chain waveguides of different lengths: Estimation of waveguide loss," Appl. Phys. Lett. **81**(9), 1714–1716 (2002).
30. D. D. Smith, G. Fischer, R. W. Boyd, and D. A. Gregory, "Cancellation of photoinduced absorption in metal nanoparticle composites through a counterintuitive consequence of local field effects," J. Opt. Soc. Am. B **14**(7), 1625–1631 (1997).

1. Introduction

Recently a surge of interest has occurred in the theory, fabrication and characterization of metamaterials: micro- and nano-structured materials with properties significantly different from their constituents, for example negative index materials [1–3] and cloaking devices [4,5]. One specific thrust focuses on the design of highly nonlinear optical materials [6] based on nanocomposites. A possible approach to obtaining a large nonlinear optical response involves taking advantage of the strong local electric fields that can be achieved in and around plasmon resonant metal nanoparticles. Since the enhancement of the third-order nonlinear susceptibility scales with the fourth power of the electric field [7–9], these resonantly enhanced local fields can dramatically increase the nonlinear response of a composite compared to that of its constituent materials. Such plasmon enhanced metal-dielectric composites have many potential optical applications; for example for enhanced two-photon fluorescence [10–12] or as optical switches [13–15], and nonlinear optical absorption [16,17]. The latter application in particular requires materials that provide significant linear transmission, while exhibiting large optical absorption under high incident irradiance. Several studies have considered the nonlinear effective medium properties of such metal-dielectric composites either experimentally or theoretically. Reports indicate that while the addition of metal leads to significant linear absorption, the composite nonlinear response can be increased with respect to the linear absorption, for example, by increasing the volume filling fraction of the nanoparticles [18,19], by increasing host refractive index [20,21], and by increasing the aspect ratio of spheroidal metal particles [22]. However, no systematic studies appear to exist on the effect of interparticle interactions in metal dielectric composites.

In the present study we investigate the nonlinear optical properties of a nanocomposite consisting of spherical silver nanoparticles arranged in a regular lattice, with a lattice spacing that is sufficiently small to prevent diffractive effects. The linear and nonlinear optical properties of these composites are studied as a function of interparticle interaction, which is

#112341 - $15.00 USD Received 3 Jun 2009; revised 5 Aug 2009; accepted 6 Aug 2009; published 10 Aug 2009
(C) 2009 OSA

varied by changing the lattice spacing while maintaining a fixed metal volume fraction. The effective optical properties are determined using numerical simulations of the three dimensional electric field distribution in the composite under plane wave excitation. We show that changing the nanoparticle arrangement significantly increases the complex nonlinear refractive index with respect to the linear absorption. The feasibility of experiments demonstrating the presence of a surface plasmon enhanced host nonlinear optical response is discussed.

2. Theory

The composite linear dielectric function ε_c of an isotropic composite with a position dependent isotropic dielectric function $\varepsilon(\omega,\vec{r})$ can be obtained based on a known linear electric field distribution of the form $\vec{E}(\omega,\vec{r})e^{-i\omega t}$ within a volume V using the following relation [23]:

$$\varepsilon_c(\omega) = \frac{\left\langle \varepsilon(\omega,\vec{r})\vec{E}(\omega,\vec{r})^2 \right\rangle_V}{\left\langle \vec{E}(\omega,\vec{r}) \right\rangle_V^2}. \tag{1}$$

Here $\vec{E}(\omega,\vec{r})$ is the position dependent complex electric field in the composite, the notation $\langle ... \rangle_V$ represents spatial averaging over volume V, and the notation $\vec{E}^2$ represents taking the dot product $\vec{E}\cdot\vec{E}$. Note that this dot product yields a complex number with a phase angle that is twice that of the original electric field vector, which will become important in this study. For simplicity of notation, frequency and position arguments are omitted in the remainder of this manuscript. The definition of the effective dielectric function given in Eq. (1) follows from the requirement of equal energy density in the effective medium and the composite. Note that identical results can be obtained by using the more common assumption of equal electric displacement in the effective medium and in the composite, as was confirmed in numerical evaluation of simulated electric field data using both approaches (data not shown). In the case of a dilute random distribution of isolated isotropic spherical nanoparticles in an isotropic host, Eq. (1) leads to the well-known Maxwell Garnett result [24]. Here we consider binary composites containing spherical inclusions of a material with an isotropic dielectric function ε_{in} embedded in a host material with an isotropic dielectric function ε_h. We limit our study to composites in which the inclusions are arranged in a rectangular lattice, and consider optical excitation with electric fields aligned with one of the principal axes of the lattice. In this specific case, Eq. (1) provides only a single diagonal element of the dielectric tensor of the anisotropic effective medium.

Analogous to the approach shown for the composite dielectric function, the effective complex third order nonlinear susceptibility of an isotropic composite $\chi_c^{(3)}(\omega)$ can be determined based on a known linear electric field distribution for the composite using the following relation [9,23,25]:

$$\chi_c^{(3)}(\omega) = \frac{\left\langle \chi^{(3)}(\omega,\vec{r})\left|\vec{E}\right|^2 \vec{E}^2 \right\rangle_V}{\left|\left\langle \vec{E} \right\rangle_V\right|^2 \left\langle \vec{E} \right\rangle_V^2} \tag{2}$$

where $\chi^{(3)}(\omega,\vec{r})$ represents a position-dependent isotropic Kerr-type third order nonlinear susceptibility at the fundamental frequency. Equation (2) was derived based on the assumption that the nonlinear polarization response is sufficiently small to be considered a perturbation on the linear response. In this study we focus on the effect of local electric field enhancement on the nonlinear refractive and absorptive properties of the composite, and ignore higher harmonic effects such as third harmonic generation. For the more general case of an anisotropic composite under monochromatic excitation, $\chi_c^{(3)}(\omega)$ must be represented by

#112341 - $15.00 USD Received 3 Jun 2009; revised 5 Aug 2009; accepted 6 Aug 2009; published 10 Aug 2009
(C) 2009 OSA

a complex fourth rank tensor. In this study we derive the effective $\chi_c^{(3)}$ only for excitation along one of the principal axes of the simulated structure, here the x-direction. In this specific case Eq. (2) provides only the tensor component $\chi_{c,xxxx}^{(3)}$, which in the following will be denoted $\chi_c^{(3)}$. Given this simplified notation, it is important to keep in mind that *the calculated susceptibilities do not represent an effective isotropic nonlinear susceptibility*, but instead represent the calculated $\chi_c^{(3)}$ for excitation with a specific electric field direction with respect to a highly symmetric structure.

For a binary composite in which the inclusion and host materials have an isotropic Kerr-type third order nonlinear susceptibility $\chi_{in}^{(3)}$ and $\chi_h^{(3)}$ respectively, it can easily be shown that Eq. (2) can be written in the following form:

$$\chi^{(3)} = f_{in} g_{in}^{(3)} \chi_{in}^{(3)} + f_h g_h^{(3)} \chi_h^{(3)} \tag{3}$$

where f_{in} is the volume fraction of the inclusion in the composite, f_h is the volume fraction of the host material given by $f_h = 1 - f_{in}$, and the factors $g_j^{(3)}$ represent susceptibility enhancement factors that satisfy the following relation:

$$g_j^{(3)} = \frac{\left\langle \vec{E}^2 \left|\vec{E}\right|^2 \right\rangle_{V_j}}{\left\langle \vec{E} \right\rangle_V^2 \left|\left\langle \vec{E} \right\rangle_V\right|^2}. \tag{4}$$

The subscript j represents either the inclusion ('in') or the host ('h'). It is important to note that the numerator is averaged over a limited volume V_j indicating the volume of the inclusion or the host respectively. From Eq. (3) the factors $g_j^{(3)}$ can be seen to represent the enhancement of the third order susceptibility contribution from host and inclusion, relative to the value expected based on a homogeneous electric field distribution throughout the volume. Note that another common definition of the enhancement factor considers the volume fraction f as part of the enhancement factor, see e.g. Ref [8]. Although the latter approach certainly provides valid results, we favor the definition shown in Eq. (3) as it more clearly highlights the contribution of the electric field redistribution to the $\chi^{(3)}$ enhancement, even for components with a small fill-fraction.

Based on the calculated composite nonlinear susceptibility $\chi_c^{(3)}$ one can obtain the composite nonlinear refractive index $\eta_{2,c} = n_{2,c} + i\kappa_{2,c}$ where $n_{2,c}$ and $\kappa_{2,c}$ represent the real and imaginary parts of the nonlinear refractive index. In highly absorptive composites the conversion from $\chi_c^{(3)}$ to the nonlinear refractive index η_2 must take into account linear loss in the composite [26] which has been shown to lead to the relation $\eta_{2,c} = (3/(4\varepsilon_0 c|\eta_c|^2))(1 - i(\kappa_c/n_c))\chi_c^{(3)}$ where ε_0 is the permittivity of vacuum, c is the speed of light in vacuum, η_c is the complex linear refractive index of the composite, and n_c and κ_c are the real and imaginary parts of η_c. The thus obtained nonlinear refractive index can be used to determine the nonlinear absorption coefficient of the composite β_c according to $\beta_c = (4\pi/\lambda)\,\kappa_{2,c}$ with λ the free space wavelength. Finally, using the calculated linear and nonlinear optical properties one can obtain the frequency dependent figure of merit for nonlinear absorption given by β/α. This figure of merit reflects the fact that high nonlinear absorption requires both a high β value as well as a low linear absorption to enable a long interaction length. This figure of merit is especially relevant in metal dielectric composites, where plasmon enhanced linear absorption will significantly affect the figure of merit.

3. Simulation geometry

For all simulations, we consider arrays of spherical silver nanoparticles embedded in a host with a frequency independent real refractive index of 1.5. This index is chosen as a typical value of commonly used host materials at visible frequencies, similar to that of for example SiO_2 (n = 1.45), many organic polymers (n ~1.4-1.6), and soda lime glass (n = 1.52). For the linear silver dielectric properties we use a surface scattering corrected Drude model fit of

#112341 - $15.00 USD Received 3 Jun 2009; revised 5 Aug 2009; accepted 6 Aug 2009; published 10 Aug 2009
(C) 2009 OSA

available literature values [27] given by $\varepsilon_{in} = \varepsilon_\infty - \omega_p^2/(\omega^2 + i\omega(\Gamma_0 + \Gamma_s))$ where $\varepsilon_\infty = 5.451$, $\omega_p = 1.474 \times 10^{16}$ rad/s, and the bulk electron scattering rate $\Gamma_0 = 8.354 \times 10^{13}$ s^{-1}. The surface scattering rate Γ_s is given by $\Gamma_s = Av_f/r = 2.8 \times 10^{14}$ s^{-1}, where A is set to 1, $v_f = 1.39 \times 10^6$ m/s is the Fermi velocity in silver, and r = 5 nm is the radius of the particle. This particle radius allows the use of sufficiently small interparticle separations to consider the composite as an effective medium in the wavelength range of interest. Note that this choice makes surface scattering the dominant contribution to the total electron damping.

Three-dimensional frequency domain electromagnetic simulations were performed using Microwave Studio [28]. For all simulations, the incident electric field is polarized along the x direction and the light propagates along the z direction. Periodic arrays of nanoparticles are simulated by considering a rectangular unit cell that contains a single 10 nm diameter Ag sphere centered in the simulation volume. The length (L_z) of the unit cell is held fixed at 30 nm, while the height (L_x) and width (L_y) are both varied while maintaining a constant unit cell volume of 30 nm × 24 nm × 24 nm. These dimensions correspond to a fixed inclusion volume fill fraction f_{in} = 0.03. An infinite array of nanoparticles is simulated by taking advantage of symmetry planes, setting the tangential electric field components to zero in the y-z plane at x = 0 and at x = $L_x/2$, and setting tangential magnetic field components to zero in the x-z plane at y = 0 and at y = $L_y/2$. In this way only a quarter of the unit cell needs to be considered in the simulations, reducing the required simulation time. Open boundary conditions are used along the z-direction. At the chosen length L_z of the simulation volume all particle-related near fields were found to be contained within the unit cell. Tetrahedral meshing is employed to simulate physically realistic electric field distributions that are virtually free of grid artifacts while using a reasonable number of mesh cells. The minimum cell size used was smaller than 1 nm on a side. The simulated linear electric field distributions were analyzed using Eqs. (1) and 2 to compute the effective linear and nonlinear composite properties for x-polarized excitation. To study the effect of interparticle interactions on the optical properties, simulations were performed for five different geometries with dimensions $L_x \times L_y$ of 12.5 × 46 nm^2, 15 × 38.4 nm^2, 24 × 24 nm^2, 38.4 × 15 nm^2, and 46 × 12.5 nm^2, corresponding to an increasing edge-to-edge interparticle separation along the x-direction of 2.5 nm, 5 nm, 14 nm, 28.4 nm, and 36 nm. These choices of longitudinal spacing L_x (along the incident electric field) and transverse spacing L_y (normal to the incident electric field) lead to significant changes of the interparticle interaction while maintaining a constant metal fill fraction. The selected interparticle separations are all significantly smaller than half the shortest optical wavelength considered, and consequently diffractive effects do not affect the optical properties of these composites.

#112341 - $15.00 USD Received 3 Jun 2009; revised 5 Aug 2009; accepted 6 Aug 2009; published 10 Aug 2009
(C) 2009 OSA

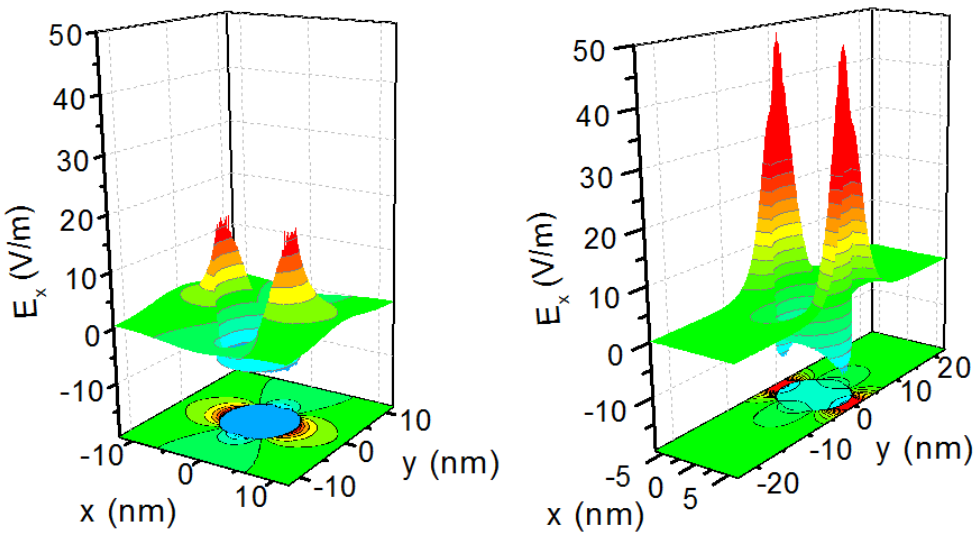

Fig. 1. Surface plot of the *x*-component of the electric field in the x-y plane for (a) the square unit cell (L_x = 24 nm) close to resonance ($\omega = 4.64 \times 10^{15}$ rad/s) and (b) a rectangular unit cell (L_x = 12.5 nm) close to resonance ($\omega = 4.0 \times 10^{15}$ rad/s). The corresponding contour graph is shown on the lower x-y plane for both cases. Contour lines are separated by 2.5 V/m.

4. Results and discussion

Figure 1(a) shows the computed electric field distribution E_x in the x-y plane for L_x = 24 nm (square arrangement of nanoparticles) under excitation with x-polarized light with a field strength of 1 V/m at a frequency close to the nanoparticle surface plasmon resonance ($\omega = 4.64 \times 10^{15}$ rad/s). The vertical scale indicates the enhancement of the lateral electric field strength (E_x) relative to the incident field, and the field is shown at the phase angle for which maximum field enhancement is observed. Contour lines are spaced 2.5 V/m apart. The field distribution around the 10 nm diameter particle appears dipolar, and shows significant field enhancement (~15 ×) near the nanoparticle surface. Figure 1(b) shows the corresponding E_x distribution for a longitudinal spacing L_x = 12.5 nm (2.5 nm edge-to-edge spacing) excited near the collective plasmon resonance of these interacting particles ($\omega = 4.0 \times 10^{15}$ rad/s). The maximum field enhancement is seen to be significantly increased to ~45 × at this reduced longitudinal interparticle spacing due to near-field interaction between adjacent particles. Consequently, an enhancement of the nonlinear optical response is expected in the regions of high field for such closely spaced geometries. Note that the geometry-related increase in peak electric field amplitude occurs predominantly in the small volume between the particles.

Figure 2 shows the linear absorption coefficient as calculated using Eq. (1) based on the simulated three-dimensional electric field data, evaluated for several frequencies of the incident plane wave. Each of the curves in Fig. 2 corresponds to one of the five interparticle spacings considered. The locations of the symbols indicate the frequency samples at which the field distribution and the corresponding optical properties were evaluated. For comparison, the dashed line labeled 'MG limit' shows the analytical result obtained using Maxwell Garnett (MG) theory for this fill fraction. The observed absorption peaks are due to the resonant excitation of approximately dipolar plasmon modes on the metal nanoparticles, leading to resonantly enhanced energy dissipation. As the longitudinal interparticle separation is reduced, a red-shift is observed in the location of the plasmon resonance compared to the Maxwell Garnett result. Conversely, at large longitudinal interparticle spacing (and small transverse interparticle spacing) a blue-shift is observed. These are well known effects that can be understood in terms of near-field interactions between neighboring metal nanoparticles [29]. Consequently these resonance must be interpreted as *collective* plasmon resonances of

#112341 - $15.00 USD Received 3 Jun 2009; revised 5 Aug 2009; accepted 6 Aug 2009; published 10 Aug 2009
(C) 2009 OSA

the lattice, rather than as individual nanoparticle plasmon resonances. The maximum linear absorption coefficient is seen to increase slightly as the longitudinal interparticle spacing is reduced. Finally, the analytical Maxwell Garnett result is seen to lie close to the numerically computed absorption coefficient for L_x = 24 nm (square arrangement), indicating that interparticle interactions are minimal in this specific geometry.

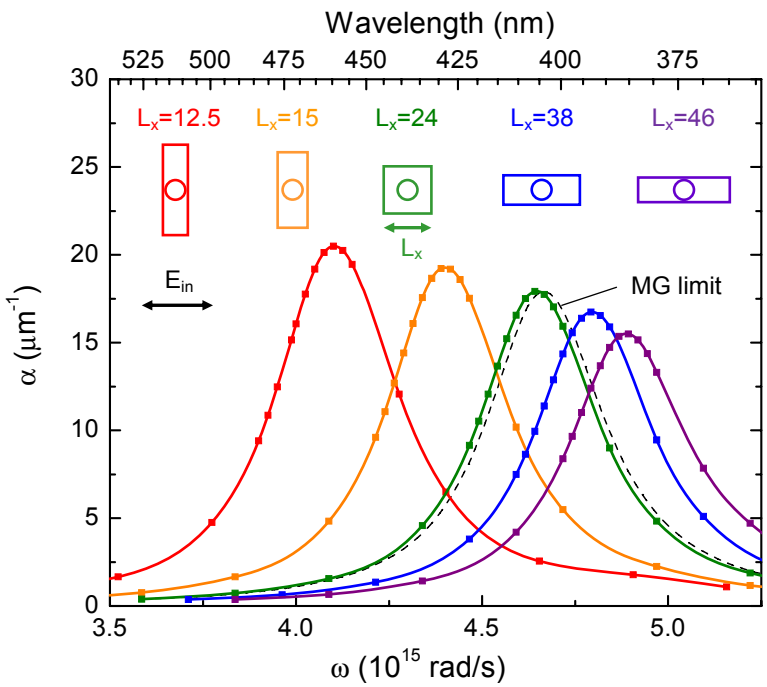

Fig. 2. Linear absorption of rectangular arrays of interacting spherical Ag particles. Symbols represent numerically computed values and are connected by a spline fit. The unit cells and the corresponding incident field polarization are shown schematically in the x-y plane.

Figure 3 shows the complex geometry-dependent nonlinear susceptibility enhancement factor $g_h^{(3)}$ calculated based on the simulated three-dimensional electric field data using Eq. (4), for different frequencies of the incident plane wave. Figure 3(a) shows the phase angle of the complex enhancement factor, and Fig. 3(b) shows the magnitude of the enhancement on a logarithmic scale. The dashed curve shows the corresponding results calculated using an analytic expression for the third order nonlinear susceptibility of composites consisting of non-interacting particles [8]. The inset in Fig. 3(b) shows the real and imaginary part of the enhancement factor on a linear scale for the non-interacting particles. Note that the analytical curve closely resembles our numerically obtained results for L_x = 24 nm in terms of magnitude, shape, and resonance frequency, showing that inter-particle interactions only weakly affect the nonlinear response in this particular geometry. For all geometries a significant nonlinear susceptibility enhancement ($g^{(3)} > 1$) is observed across a large frequency bandwidth near the plasmon resonance, with maximum enhancement occurring near the surface plasmon resonance of the structure. As the longitudinal interparticle spacing is reduced, the magnitude of the enhancement is seen to increase by more than an order of magnitude. Apparently the field enhancement obtained at small interparticle spacing results in a net increase of $g^{(3)}$, despite the fact that the enhancement occurs only within a small volume. While interparticle interaction does contribute to the enhancement, the field enhancement obtained due to the plasmon resonance provides the main contribution to the observed enhancement factors. The resonant nature of the enhancement has an important consequence: as can be seen in Fig. 3(a), the phase angle of the enhancement factor increases from

#112341 - $15.00 USD Received 3 Jun 2009; revised 5 Aug 2009; accepted 6 Aug 2009; published 10 Aug 2009
(C) 2009 OSA

approximately 0° to 360° as the frequency is increased from below the plasmon resonance frequency to well above the resonance frequency. This behavior can be understood by realizing that near resonance the local electric fields inside and just outside the nanoparticles occur with respectively a –90° and + 90° phase delay with respect to the incident field. As can be seen in Eq. (4), the phase of the numerator of the enhancement factor scales with E^2, and consequently the 90° phase difference of the linear fields on resonance lead to a 180° phase difference of the numerator in Eq. (4) compared to the phase of the average field. The complex nature of the enhancement indicates that in the presence of metal nanoparticles, a Kerr-type positive nonlinear refractive host can act as a nonlinear absorber, a negative nonlinear refractive medium, or a saturable absorber, depending on the frequency used [16,17]. Note that in experiments on metal-dielectric composites these effects may be overshadowed by nonlinearities introduced by the metal nanoparticles.

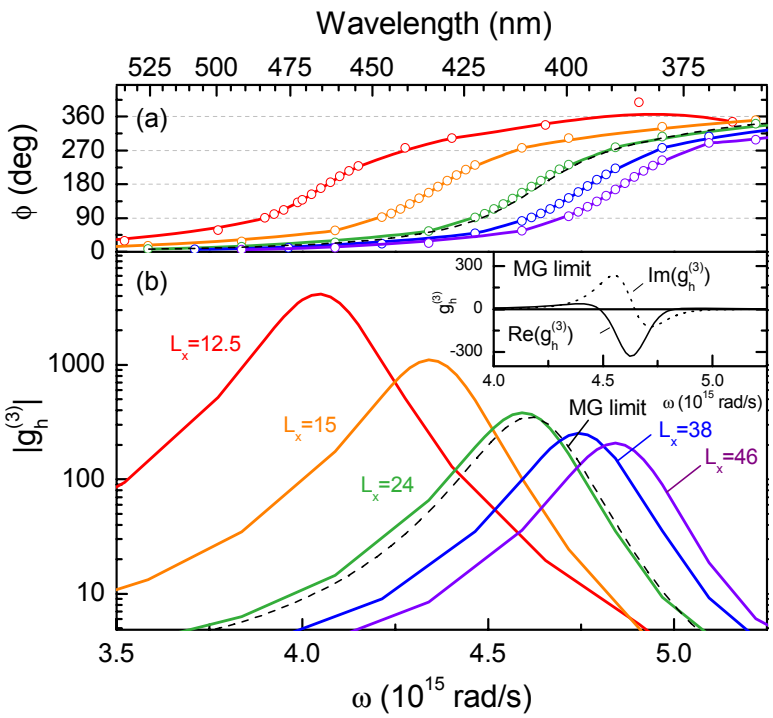

Fig. 3. Complex geometry-dependent nonlinear susceptibility enhancement factor $g_h^{(3)}$ for different frequencies of the incident plane wave, showing (a) the phase angle of the complex enhancement factor, and (b) the magnitude of the enhancement on a logarithmic scale. The dashed curves show the corresponding analytically obtained results for non-interacting particles (MG limit). The inset shows the real (solid line) and imaginary (dotted line) enhancement factors on a linear scale for the case of non-interacting particles.

Figure 4 shows the phase (Fig. 4(a)) and magnitude (Fig. 4(b)) of the geometry-dependent nonlinear susceptibility enhancement factor $g_{in}^{(3)}$ of the inclusion, based on the same simulated three-dimensional electric field data used to generate Fig. 3. Note that while the phase dependence on frequency appears virtually identical to that observed in Fig. 3(a), the curves shown in Fig. 4(a) are in fact independently calculated values based on the *internal* electric fields, as opposed to the external electric fields that were used to generate Fig. 3(a). The dashed curves represent the corresponding analytical result for this fill fraction. This analytical result relies on a different equation than the one used in Fig. 3, since it also considers the internal fields [8]. In the limit of weak interparticle interaction (L_x = 24 nm), the magnitude of the enhancement $g_{in}^{(3)}$ is seen to be significantly larger than that of $g_h^{(3)}$ observed in Fig. 3. This is due to fact that the internal field enhancement that contributes to $g_{in}^{(3)}$ occurs

#112341 - $15.00 USD Received 3 Jun 2009; revised 5 Aug 2009; accepted 6 Aug 2009; published 10 Aug 2009
(C) 2009 OSA

throughout the entire volume of the particle, while the external field enhancement that contributes to $g_h^{(3)}$ occurs only in a small fraction of the host volume. In stark contrast with the observations made in Fig. 3, the magnitude of the nonlinear susceptibility enhancement of the inclusion is found to be nearly independent of interparticle separation. This very different behavior is due to the fact that the internal field distribution is relatively unaffected by changes in the interparticle separation.

Using the calculated linear effective dielectric function and nonlinear susceptibility enhancement factors $g_j^{(3)}$ it is now possible to evaluate the influence of the geometry-dependent field enhancement on the figure of merit for nonlinear absorption. The figure of merit is given by β_c/α_c, where β_c is the nonlinear absorption coefficient of the composite. The figure of merit indicates the inverse of the irradiance required to achieve a nonlinear absorption coefficient equal to the linear absorption coefficient. For the following analysis the silver nonlinear response is approximated by a Kerr-type response with $\chi_{in}^{(3)} = i*10^{-10}$ esu ($1.75i \times 10^{-17}$ V^2/m^2), while the host is assumed to be nonlinearly refractive with $\chi_h^{(3)} = 10^{-14}$ esu (1.75×10^{-21} V^2/m^2). For clarity of presentation these values are assumed to be frequency independent near the nanoparticle resonance. Note that while metal nonlinear optical properties are often described in terms of an effective Kerr nonlinearity, the underlying physical mechanisms include non-Kerr type effects such as Fermi smearing and thermal nonlinearities. Consequently, the metal contribution to the composite nonlinearity in real-world experiments may not reproduce the exact functional form derived here, however the predicted trends are expected to be observable.

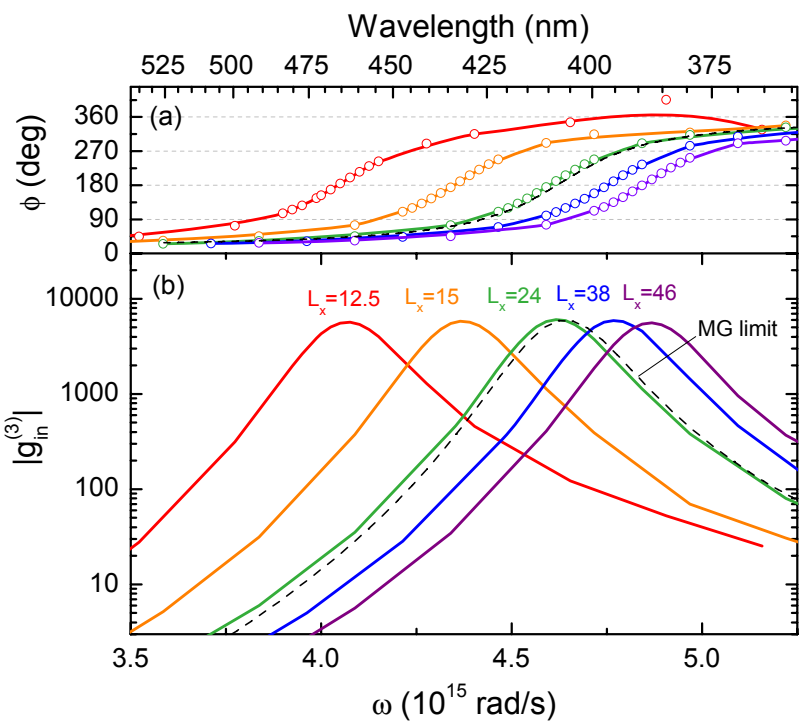

Fig. 4. Complex geometry-dependent nonlinear susceptibility enhancement factor $g_{in}^{(3)}$ for different frequencies of the incident plane wave, showing (a) the phase angle of the complex enhancement factor, and (b) the magnitude of the enhancement on a logarithmic scale. The dashed curves show the corresponding results for non-interacting particles (MG limit).

The total figure of merit for nonlinear absorption can be shown to be separable into a host contribution and an inclusion contribution. Figure 5(a) shows the host contribution to the figure of merit of the composite as a function of geometry. Despite the fact that a nonlinear

#112341 - $15.00 USD Received 3 Jun 2009; revised 5 Aug 2009; accepted 6 Aug 2009; published 10 Aug 2009
(C) 2009 OSA

refractive host is assumed, a positive figure of merit for nonlinear *absorption* is observed across a significant frequency range due to the complex nature of the susceptibility enhancement factor near the plasmon resonance of the structure. As the longitudinal interparticle spacing is decreased from 46 nm to 12.5 nm, the peak figure of merit is seen to increase by more than an order of magnitude. This increase follows from the observed large increase in the effective nonlinear susceptibility (Fig. 3) due to near-field coupling between adjacent particles accompanied by additional field enhancement and confinement (Fig. 1), combined with the relatively small change in peak absorption coefficient as the interparticle spacing is modified (Fig. 2). These results demonstrate that while the presence of the metal nanoparticles does introduce significant absorption, the nonlinear optical absorption performance of a thin metal-dielectric composite can be improved significantly by modifying the spatial distribution of the metal. Figure 5(b) shows the contribution of the inclusion to the overall figure of merit of the composite as for the same geometries. The entirely imaginary $\chi_{in}^{(3)}$ assumed for the metal is seen to lead to a *negative* figure of merit for nonlinear absorption, indicative of a composite that exhibits saturable absorption. Experimental studies of metal-dielectric composites indeed show saturable absorption near the plasmon resonance [17,30]. As the longitudinal interparticle spacing is decreased, the magnitude of the figure of merit is seen to decrease slightly due to the observed weak increase in linear absorption as the longitudinal interparticle spacing is decreased (Fig. 2), and partly due to an additional frequency dependence introduced by the factor $1/\lambda$ in the conversion from $\chi^{(3)}$ to β.

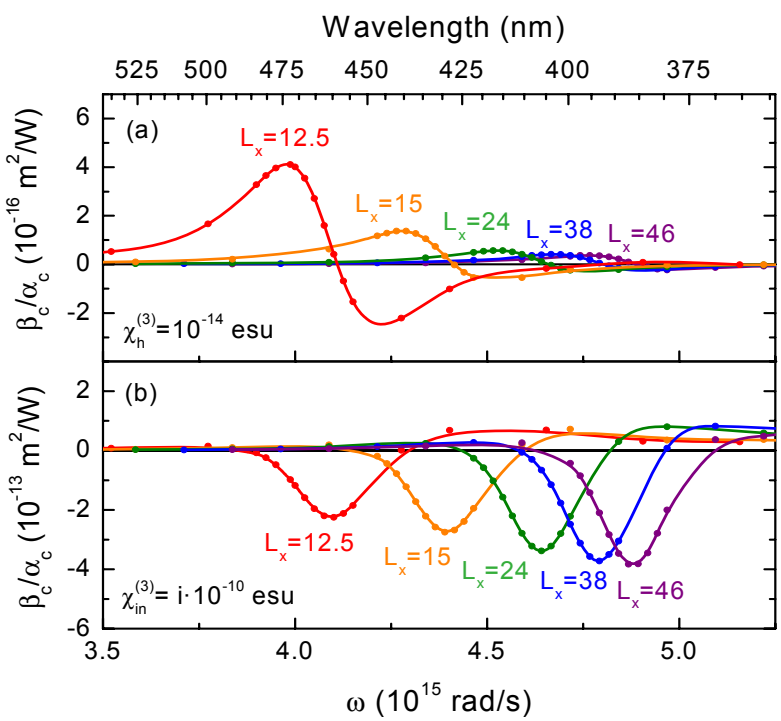

Fig. 5. Contributions to the figure of merit of the composite as a function of geometry considering separately (a) a nonlinear host, and (b) a nonlinear inclusion.

It is important to note that the specific example shown in Fig. 5 assumes a weak nonlinear contribution, using equations derived to first order in nonlinear polarization. This assumption will cease to be valid in cases where a significant change in total absorption is achieved relative to the already present metal-induced absorption. Consequently the complete evaluation of plasmon-enhanced nonlinear absorbers will require calculations that go beyond the first order perturbation approach. Secondly, the high irradiances required to achieve

#112341 - $15.00 USD Received 3 Jun 2009; revised 5 Aug 2009; accepted 6 Aug 2009; published 10 Aug 2009
(C) 2009 OSA

measurable changes in the absorption will induce significant heating and possibly melting and sintering of metal nanoparticles, adding an experimental challenge to studies of these effects, particularly for relatively slow measurements involving nanosecond pulses. Note also that for the values of $\chi_{in}^{(3)}$ and $\chi_h^{(3)}$ chosen in this example the metal nonlinear response provides by far the dominant contribution to the figure of merit. While the values used here were chosen mainly for illustrative purposes, their magnitudes are not unrealistic, and consequently the experimental observation of plasmon enhancement of nonlinear refractive or absorptive host properties are expected to be challenging. A potentially mitigating factor is that our choice of nanoparticle diameter as discussed previously leads to a significant predicted contribution of surface scattering to the total electronic damping. Consequently experimental studies using larger particles may produce a significantly stronger nonlinear optical response due to a reduction in surface scattering. Further optimization of particle arrangement and particle shape may lead to an experimentally observable enhancement of host-related nonlinear optical refractive and absorptive effects in real metal-dielectric composite materials.

5. Summary and conclusions

The effect of interparticle spacing on the linear and nonlinear optical properties of periodic metal-dielectric nanocomposites was discussed. Under the assumption that the materials exhibit a third-order Kerr type nonlinearity, it is shown that a reduced interparticle spacing along the incident field direction can lead to a significantly increased composite nonlinear optical response at frequencies near the plasmon resonance, while leaving the maximum linear optical absorption largely unaffected. These two findings lead to the observation of an enhanced figure of merit for nonlinear absorption by a nonlinear refractive host.

Acknowledgements

We would like to thank Prof. David G. Stroud for helpful discussions. This material is based upon work supported by the U. S. Army Research Office under contract/grant number 50372-CH-MUR.

#112341 - $15.00 USD Received 3 Jun 2009; revised 5 Aug 2009; accepted 6 Aug 2009; published 10 Aug 2009
(C) 2009 OSA